European Polymer Journal 105 (2018) 150–157

Contents lists available at ScienceDirect

European Polymer Journal

journal homepage: www.elsevier.com/locate/europolj

Carbon nanotube mediated miscibility of polyhydroxyalkanoate blends and chemical imaging using deuterium-labelled poly(3-hydroxyoctanoate)

Robert A. Russell[a,b,*], L. John R. Foster[c], Peter J. Holden[a]

[a] National Deuteration Facility, Australian Nuclear Science and Technology Organisation, Locked Bag 2001, Kirrawee DC, NSW 2232, Australia
[b] School of Biotechnology & Biomolecular Sciences, University of New South Wales, Sydney, NSW 2052, Australia
[c] Bio/polymer Research Group, Department of Chemistry, University of Alabama in Huntsville, Huntsville, AL 35899, USA

ARTICLE INFO

Keywords:
Bionanocomposite
Deuteration
Miscibility

ABSTRACT

Biopolymers have potential as scaffolds supporting regrowth of damaged tissues, however their material properties may limit the range of applications. Blending polymers with different thermomechanical properties has been demonstrated to extend the range of possible applications for polyhydroxyalkanoate (PHA) polymers, while the addition of nanoparticles can be used to modulate miscibility which influences strength and flexibility of the blend. Here we report on the blending of Poly(3-hydroxybutyrate) and Poly(3-hydroxyoctanoate) which possess different thermomechanical properties, and the effect of single wall carbon nanotubes (SWCNT) on their miscibility, electrical conductivity and thermomechanical performance. The apparent perturbation of phase boundaries in nanocomposite films observed by Scanning Electron Microscopy (SEM) was complemented by chemical mapping of film cross sections containing a deuterium-labelled poly(3-hydroxyoctanoate) phase in the blend using Infrared Microspectroscopy (IRM), suggesting increased miscibility due to nanoparticle addition. The electrical percolation threshold in nanocomposite films was observed between 0.5 and 1 wt% SWCNT, where the surface resistivity was reduced by eight orders of magnitude compared to the insulating polymer blend. Addition of SWCNT did not impact significantly on mechanical properties of films containing up to 2.5 wt % SWCNT. A solvent cast bionanocomposite film containing optimally 1 wt% SWCNT yielded a material with improved electrical conductivity compared to the SWCNT-free blend and which supported growth of Olfactory Ensheathing Cells, providing a basis for developing biopolymer scaffolds capable of conducting electrical stimulation.

1. Introduction

Polyhydroxyalkanoates (PHAs) are a family of biopolyesters commonly produced by microorganisms utilising a variety of carbon based substrates to synthesise short chain length (*scl*) and medium chain length (*mcl*) PHAs [1,2]. Poly(3-hydroxybutyrate) (PHB) is the most commonly studied and applied member of the PHA family but its application is often limited by its brittle and crystalline nature [3,4]. Despite this, there are many reports on the usefulness of PHAs in biomedical devices and applications [5–8]. Blending PHB with *mcl*-PHAs or unrelated polymers may be employed to modulate material properties, however the drawbacks of blending immiscible polymers include mechanical weaknesses at fracture due to weak adhesion between polymer chains at the phase interface, which may be exacerbated by large domain size [9–13]. Theoretical studies have suggested that nanorods may be used as an effective emulsifying agent in such polymer solutions, slowing down the phase separation process and reducing the length scale of the material domains upon evaporation [14]. Failures at the interface between polymer phases could be ameliorated by addition of carbon nanotubes, where the diffusion of chain segments across the interface is apparently enhanced and the propagation of cracking reduced. In a study of melt blended Poly(ε-caprolactone)/Polylactide, Multi Wall Carbon Nanotubes (MWCNT) were found to be selectively dispersed in the matrix phase and at the interface between two polymer phases [15]. More recently, MWCNT have been shown to reduce the macromolecular mobility of immiscible blend components, with selective localization of the nanoparticles in one of the polymer phases [16,17]. This selective dispersion of conductive nanoparticles, compared to more homogeneous distribution in monophasic composites, has been demonstrated to improve electrical conductivity, especially where the nanoparticles were confined to the interface between the polymer phases [18,19].

Miscibility of *scl*-/*mcl*-PHA solvent cast blends has been probed by Scanning Electron Microscopy (SEM) and thermomechanical analysis

* Corresponding author.
E-mail address: rar@ansto.gov.au (R.A. Russell).

https://doi.org/10.1016/j.eurpolymj.2018.05.031
Received 10 April 2018; Received in revised form 21 May 2018; Accepted 25 May 2018
Available online 26 May 2018

[20]. We have previously demonstrated chemical imaging of deuterium-labelled poly(3-hydroxyoctanoate) (D-PHO) using Infrared Microspectroscopy (IRM) to reveal phase separation in films containing equimolar amounts of PHB and PHO [20,21]. We hypothesized that addition of SWCNT to these polymer blends would enhance miscibility and therefore result in a biomaterial with more desirable thermomechanical properties that may prove suitable as scaffolds for tissue regeneration and engineering. Furthermore, an effective dispersion of the nanoparticles was anticipated to increase electrical conductivity in the films, opening opportunities for propagation of electrical stimulation through the material. This would support their potential as a scaffold in nerve repair, as reported in the application of electrical stimulus through biomaterial to enhance neural cell viability, proliferation and neurite outgrowth [22–26].

2. Materials and methods

2.1. Material and reagents

Chemicals, including PHB, were obtained from Sigma-Aldrich (St. Louis, MO, USA) and used as received. SWCNT nominally 1 nm diameter and 1–2 μm in length were obtained from CheapTubes.com. PHO and D-PHO were prepared and characterized as previously reported [21,27,28]. Briefly, the PHO biopolymer was produced by fed-batch biosynthesis using *Pseudomonas oleovorans* (ATCC 29347) in minimal medium with octanoic acid as the sole carbon source. Deuterated PHO (D-PHO) was biosynthesized from deuterated carbon source (octanoic acid-d_{15}, 98% D by ^{1}H NMR). Crude polymers were extracted from the freeze-dried biomass into chloroform and precipitated by addition of cold methanol. Polymers were then dried under vacuum to remove traces of solvent.

2.2. Preparation of film blends and nanocomposites

Films of PHA blends were prepared by solvent casting into PTFE-lined petri dishes (Welch Fluorocarbons, USA). Equal masses of PHB and PHO (or D-PHO) were dissolved in chloroform in sealed vials with stirring at 400 rpm and 60 °C. SWCNT were suspended in chloroform with stirring and aliquots were added to PHB/PHO solutions to achieve final concentrations from 0.1 to 10 wt% SWCNT. The nanocomposite mixtures were sonicated for 6 min at 3 W using a probe tip (Misonix 3000, NY, USA), with a 30 s on/off cycle to permit heat dissipation. Chloroform was slowly evaporated from a glass-covered petri dish to form films of even consistency, 75 ± 25 μm thickness as measured by digital calipers.

2.3. Infrared Microspectroscopy

Films containing a deuterated polymer phase (D-PHO) were microtomed to obtain sections (ca. 5 μm thickness) and mounted onto CaF_2 discs (Crystan Ltd., Poole, UK). The film cross sections were examined in transmission mode using a Bruker FT-IR spectrometer attached to a Hyperion 3000 IR microscope equipped with a 64 × 64 pixel focal plane array (FPA) imaging detector. With the microscope reflective IR Cassegrain objective and condenser (15×, 0.4 N.A.), each detector field of view corresponded to ca. 170 μm^2 on the sample. Larger sample areas were investigated by compiling several of these frames. All data were recorded using Bruker OPUS version 6.5 software, and data analysis was performed using Bruker OPUS 7.0 imaging software.

2.4. Scanning Electron Microscopy

SEM images of polymer blends were collected using an FEI Nova NanoSEM 230 operating at 3 kV or Hitachi S3400-N at 5 kV. Samples were prepared by cryomicrotoming (Leica EM FC6 Cryo-Ultramicrotome) or freeze-fracturing after plunging into liquid nitrogen for at least 30 s prior. The exposed face of the film cross section was mounted on a stub using conductive carbon tape and coated with a layer of platinum (ca. 5 nm thick) prior to placing into the microscope chamber.

Cell growth on PHB/PHO films was tested using Murine Olfactory Ensheathing Cells (OECs) extracted from 5-week-old Wistar rats (University of NSW ACEC number-06/53A) and cultivated on Dulbecco's Modified Eagle's Medium (DMEM, Gibco-Invitrogen, Australia) containing 10% foetal bovine serum (FBS, Gibco-Invitrogen, Australia), 250 μg/mL penicillin, 250 μg/mL streptomycin and 1 μg/mL fungizone-amphotericin B (Gibco-Invitrogen, Australia). Cells were washed in PBS buffer then resuspended in fresh DMEM containing 10% FBS and inoculated at approximately 10^4 cells/well into multi-well plates containing nanocomposite films. Cells were incubated for 3–5 days prior to fixing in 2.5% glutaraldehyde solution and dehydrated in increasing concentrations of ethanol. Samples in 100% ethanol were then dried in liquid CO_2 at the critical point prior to for SEM analysis.

2.5. Resistivity measurements

Surface resistance of nanocomposite films was measured using a resistance meter (PRS-812) with concentric ring probe (PRF-912B) from Prostat Corporation (Bensenville, IL, USA). Average resistance was calculated from replicate measurements and from areas of different appearance in non-homogenous films where applicable (n = 5).

2.6. Thermomechanical measurements

Thermal properties were investigated by differential scanning calorimetry (DSC) using a DSC1 StarE with intracooler (Mettler-Toledo AG, Switzerland). Samples ca. 5 mg in aluminium pans were heated to 200 °C at 10 °C/min to remove thermal history then cooled to −70 °C at 10 °C/min to determine crystallisation temperature (T_c) and the degree of crystallinity X_c (%) of the PHB phase. Melting temperatures (T_m) and glass transitions (T_g) were determined from second heating run to 200 °C. Crystallinity was calculated using equation (1), where ΔH_m is the melting enthalpy and ΔH_{100} is the theoretical enthalpy of fusion for 100% crystalline PHB (146 J/g) [29].

$$X_c = \frac{\Delta H_m}{\Delta H_{100}} \times 100 \quad (1)$$

Mechanical testing of rectangular film pieces ca. 10 × 30 mm was performed using an Instron 5543 tensiometer (Canton, USA). Samples were held between two pneumatic clamps positioned at 25–30 mm with a cross-head speed of 20 mm/min. Tensile strength and extension to break were calculated (n = 5) using Bluehill software (v4.2, Instron, Canton, USA).

3. Results and discussion

3.1. Chemical mapping of protonated/deuterated PHA blend miscibility

Solvent cast films of PHB and PHO blends have previously been shown to be immiscible using SEM and IRM techniques, particularly around equimolar ratios [20,21]. Here we investigated the addition of SWCNT to blends of equimolar PHB and D-PHO, using IRM to probe the effect on miscibility. The chemical maps obtained through the film cross sections show areas of high (pink/red) and low (blue/green) infrared absorbance corresponding to C—H stretching vibrations (2800–3050 cm^{-1}) primarily from the PHB phase, and C—D stretching vibrations (2050–2200 cm^{-1}) in the D-PHO phase respectively. The solvent cast blend without addition of nanoparticles shows domains of high C—H absorbance corresponding to low C—D absorbance, and *vice versa* (Fig. 1), indicating phase separation of PHB and D-PHO in the

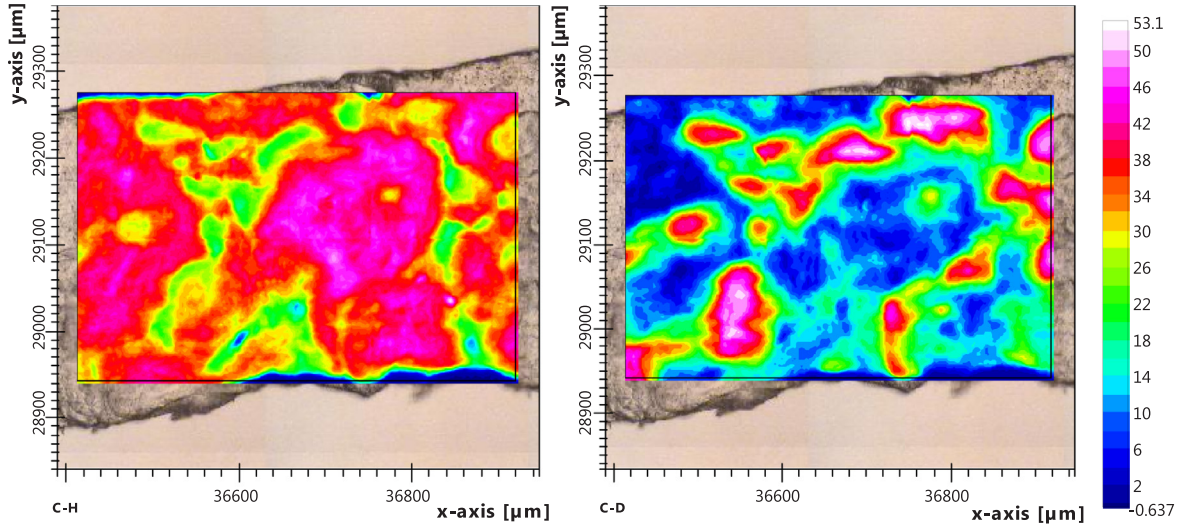

Fig. 1. False-colour IR absorbance contour maps of equimolar PHB/D-PHO film cross section, overlaid on visual image. C—H stretching vibration (left) and C—D stretching vibration (right).

solvent-cast film.

The film containing 0.1 wt% SWCNT showed separate domains of PHB and D-PHO absorbance, but with greater overlap than in the blend without nanoparticle addition (Fig. 2). The film containing 1 wt% SWCNT (Fig. 3) showed similar separation of protonated and deuterated polymer phases, but displayed broader areas of intermediate absorbance intensity suggesting greater miscibility. When the nanoparticle loading was increased to 5 wt% SWCNT, both polymers appeared to be more dispersed throughout the film cross section (Fig. 4). Domains of D-PHO were comparatively less apparent and tended to overlap with areas of high PHB absorbance, indicating a higher degree of miscibility in this nanocomposite. These results are consistent with earlier reports that nanoparticles such as carbon nanotubes perturb the phase boundaries and increase miscibility in polymer blends [12]. At this high nanoparticle loading, aggregates of SWCNT appeared as small domains of low absorbance (dark blue in C—H and C—D chemical maps).

Due to the thickness of the cross sections, the chemical maps may show some overlap of phases due to IR transmission through the films. Recent work by Rickard et al. described the chemical mapping of protonated/deuterated films cryomicrotomed to 300 nm thin sections, which would minimize this effect [30]. Furthermore, their use of AFM-IR enabled high spatial resolution across the phase boundaries. Application of this technique to probing PHA composite films presented here may further enhance resolution of phase boundary effects in polymer-nanoparticle interactions.

3.2. SEM analysis of film cross sections

A cross section of the solvent cast PHB/PHO film without SWCNT, when cut by cryomicrotome, showed a continuous surface without phase differentiation, but with occasional voids (Fig. 5a). In contrast, the freeze-fractured surface of the PHB/PHO film showed phase-separated domains, with sharp boundaries between areas (examples indicated by white arrows in Figs. 5b and 6a) that can be attributed to the soft and elastomeric PHO compared to the more crystalline PHB phases. Some of these domains protruded outward from the fractured surface, while others appeared as depressions. The domain sizes of several tens of µm agrees with the IRM data previously reported in PHB/D-PHO blends [21].

When SWCNT were incorporated into the PHO/PHB blended films, the domains attributed to PHO were still apparent, however the boundaries between domains were comparatively less defined. Addition of 0.1 wt% SWCNT showed a porous PHB matrix in the freeze-fractured

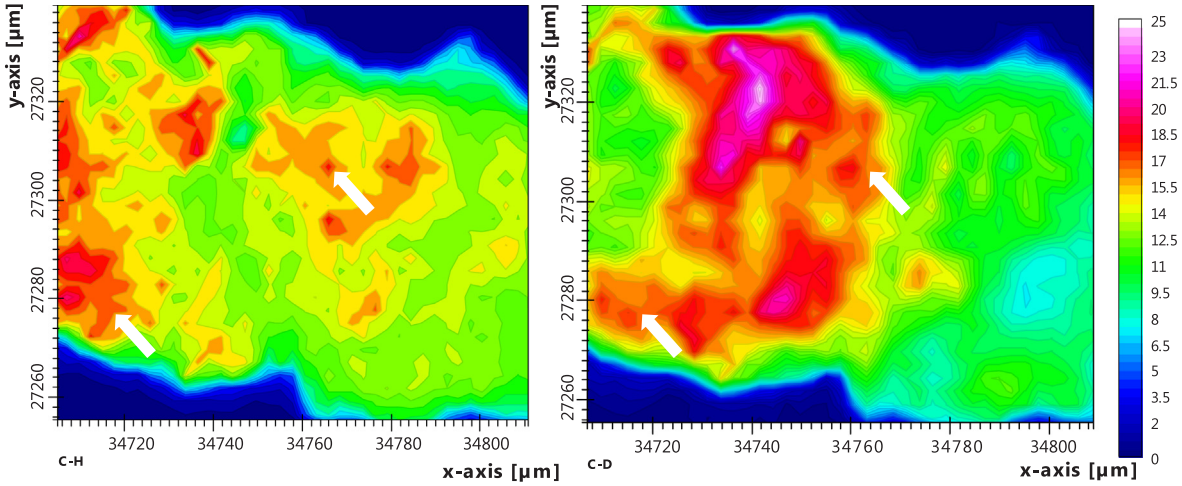

Fig. 2. False-colour IR absorbance contour maps of equimolar PHB/D-PHO + 0.1 wt% SWCNT film cross section. C—H stretching vibration (left) and C—D stretching vibration (right). *White arrows* indicate areas of phase overlap.

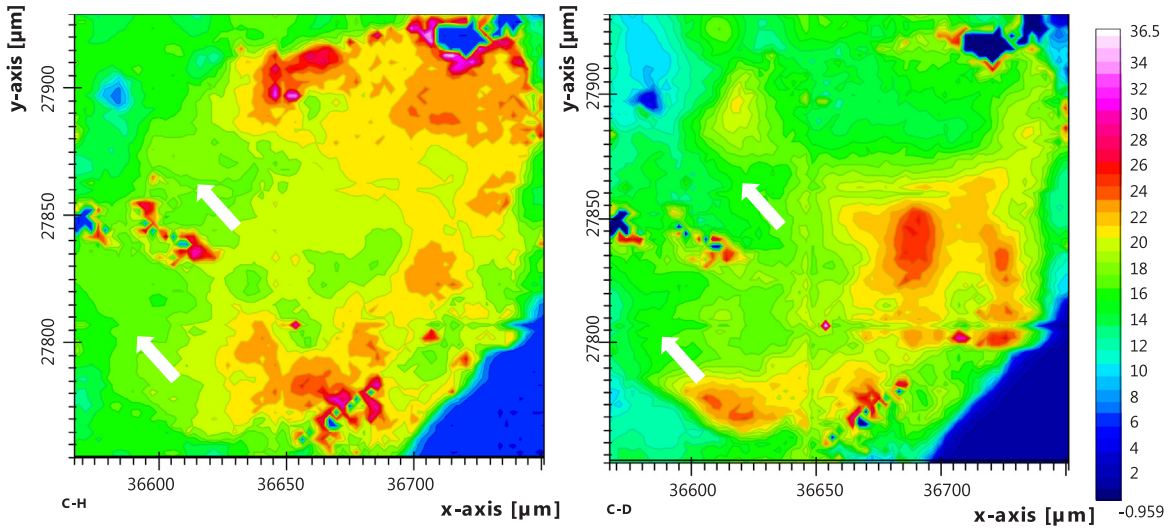

Fig. 3. False-colour IR absorbance contour maps of equimolar PHB/D-PHO + 1 wt% SWCNT film cross section. C—H stretching vibration (left) and C—D stretching vibration (right). *White arrows* indicate areas of intermediate intensity.

cross section similar to the SWCNT-free blend, but an absence of phase boundaries with the elastomeric PHO suggested greater miscibility was achieved (Fig. 6a). The freeze-fractured film section containing 1 wt% SWCNT showed a comparatively larger pore structure and domains of PHB and PHO without distinct phase boundaries (Fig. 6b). Addition of 5 wt% SWCNT resulted in more regular cavities such as those seen in the blend, however the PHO phase appeared well dispersed into the porous PHB and largely miscible through the freeze fractured cross section (Fig. 6c). These results are consistent with the observations from the IR chemical maps, in that the nanoparticles perturbed the phase boundary and produced overlap between the phases but did not result in complete miscibility. It is likely the SWCNT slowed the separation of polymer phases during evaporation of the solvent, but their influence on crystallite formation, as reported in the thermal analysis, may also play an important role in the apparent increase in miscibility. Furthermore, phase separation between immiscible polymers has been reported as favouring partitioning of nanoparticles either between phases or preferentially with a phase. This may lead to greater electrical conductivity compared to films with an even distribution of SWCNT or containing only one polymer phase [18,19].

3.3. Resistivity measurements

Relatively high resistivity, exceeding 10^{11} Ω, was observed in PHB and PHB/PHO blended solvent cast films, without carbon nanotubes (Fig. 7), as expected for insulating PHA polymers and consistent with previous reports [31–33]. Resistivity was not affected by the addition of 0.1 wt% SWCNT, and remained high in the case of PHB up to 1 wt% SWCNT loading. While a small decrease in surface resistance was observed in PHB/PHO films containing 0.5 wt% SWCNT, this was insufficient to produce a consistent conductive network in the polymer matrix. The percolation threshold, above which the network of carbon nanotubes formed a pathway for electric current to pass through the film, was observed at a loading of 1 wt% SWCNT in the blend, in which the surface resistivity decreased 5 orders of magnitude to less than 10^{6} Ω. The phase separation in the blend likely induced some partitioning of nanoparticles between phases, however the ultra-low percolation thresholds reported for PLLA/PCL/MWCNT and epoxy/MWCNT composites [18,19], due to selective distribution of nanoparticles at the interface between polymer phases, were not observed here. Nevertheless, similar compositions of poly(3-hydroxybutyrate-co-3-

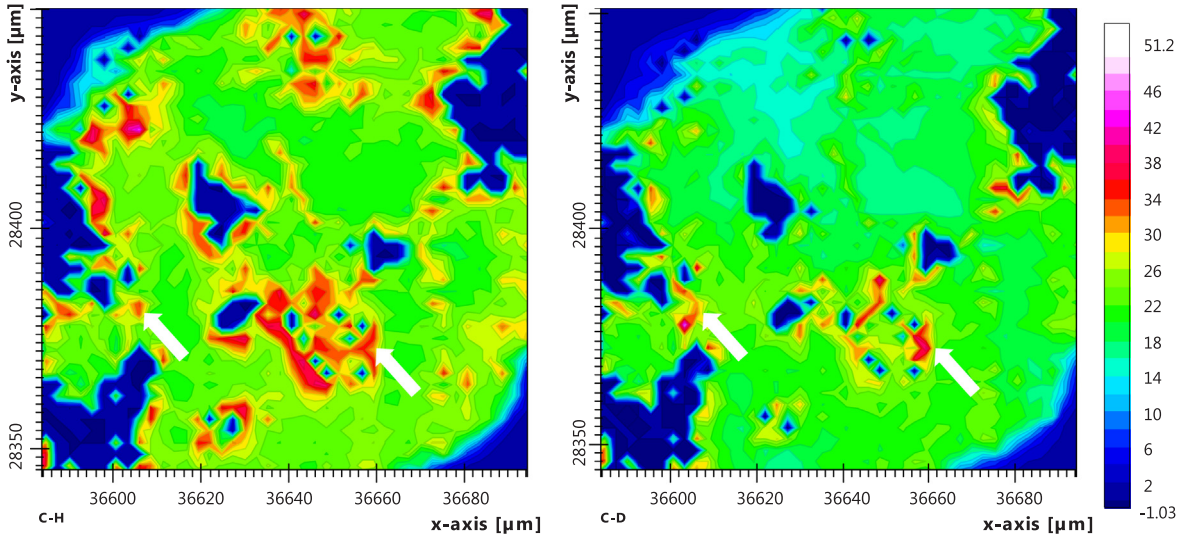

Fig. 4. False-colour IR absorbance contour maps of equimolar PHB/D-PHO + 5 wt% SWCNT film cross section. C—H stretching vibration (left) and C—D stretching vibration (right). *White arrows* indicate areas of phase overlap.

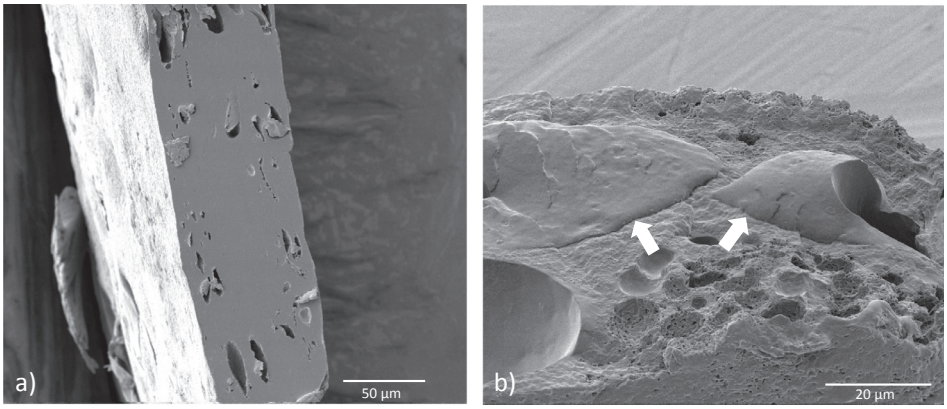

Fig. 5. SEM images of equimolar PHO/PHB blends (a) cryomicrotomed; (b) freeze-fractured, tilted to highlight polymer domains. *White arrows* indicate phase boundaries between polymer domains.

hydroxyhexanoate) co-polymer with 0.3 wt% to 1 wt% MWCNT have been reported to enhance electrical conductivity and promote proliferation and activity of mammalian cell cultures [33,34].

Additional SWCNT loading up to 10 wt% further reduced the surface resistance to less than 10^4 Ω – a likely consequence of more extensive contact between nanoparticles enhancing electrical conductivity. Reports of CNT loading in the literature generally show a percolation threshold for electrical conductivity around 1–2 wt%, however Dufresne et al. showed resistivity continued to decrease with CNT loading up to 15 wt% [35]. The comparatively greater loading of SWCNT required in the PHB homopolymer films to exceed the percolation threshold (2.5 wt%) suggests a more dispersed nanoparticle distribution when compared to their distribution in the relatively immiscible PHB/PHO blended films. The percolation threshold for PHB/SWCNT films reported here is somewhat higher than the percolation thresholds reported for PHO/graphene (0.5–1 wt%) and PHB/MWCNT or SWCNT (0.2 wt%) films [31,36], and the variability observed above the percolation threshold may be due to aggregation of the SWCNT during crystallization of the PHB film.

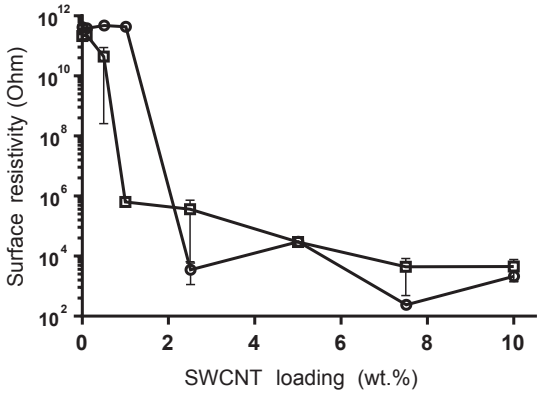

Fig. 7. Resistivity of nanocomposite film surfaces: PHB (circles) and equimolar PHB/PHO (squares) containing SWCNT. $N = 5$, error bars represent standard error of the mean.

3.4. Thermomechanical properties

Miscibility of PHB/PHO blends has previously been probed using DSC to determine thermal events during heating of solvent cast and quenched films [20]. The distinct glass transition temperatures suggested that PHB and PHO were immiscible in the amorphous state, while the slight decrease in melting temperature (T_m) of the PHB phase was postulated to relate to smaller PHB crystallites. In this study glass transitions of PHO and PHB phases were observed at approximately −40 °C and 5 °C, respectively (Fig. 8). The transitions remained distinct across the range of films with SWCNT loadings, indicating the presence of separate polymer phases.

Heating and cooling cycles of equimolar PHB/PHO blends with SWCNT loadings up to 10 wt% were analysed to determine the effect of SWCNT on melting temperatures and crystallinity of the PHB phase (Table 1). Films of PHB/PHO containing SWCNT showed little variation in melting temperature of the PHB phase ($T_{m(PHB)}$), but an increasing temperature of crystallisation ($T_{c(PHB)}$) with SWCNT loading. This suggested that SWCNT provided nucleation sites in the PHB phase, promoting crystallite formation upon cooling from the melt. The crystallinity of films fabricated from equimolar PHB/PHO blends with nanocomposites ranged from 42 to 52%, but was apparently independent of nanoparticle loading.

Solvent cast films fabricated from blends of PHB and PHO have

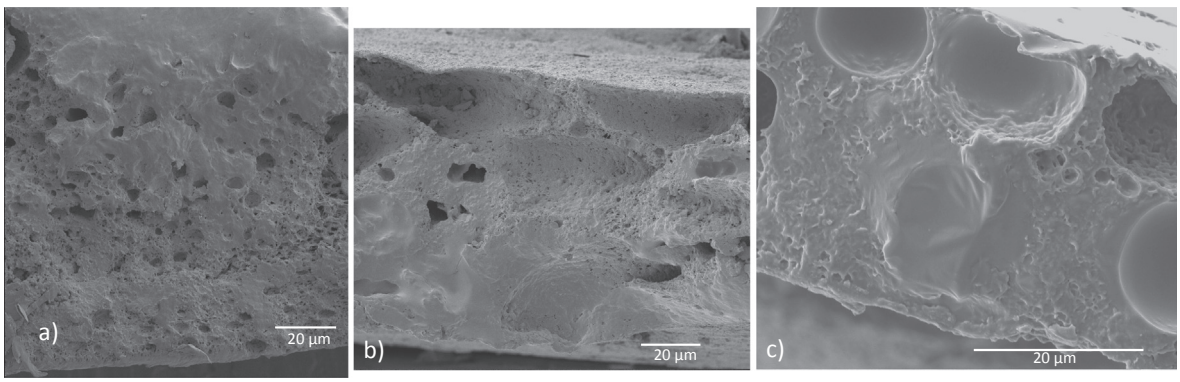

Fig. 6. SEM images of freeze-fractured equimolar PHB/PHO films containing: (a) 0.1 wt% SWCNT; (b) 1 wt% SWCNT; (c) 5 wt% SWCNT.

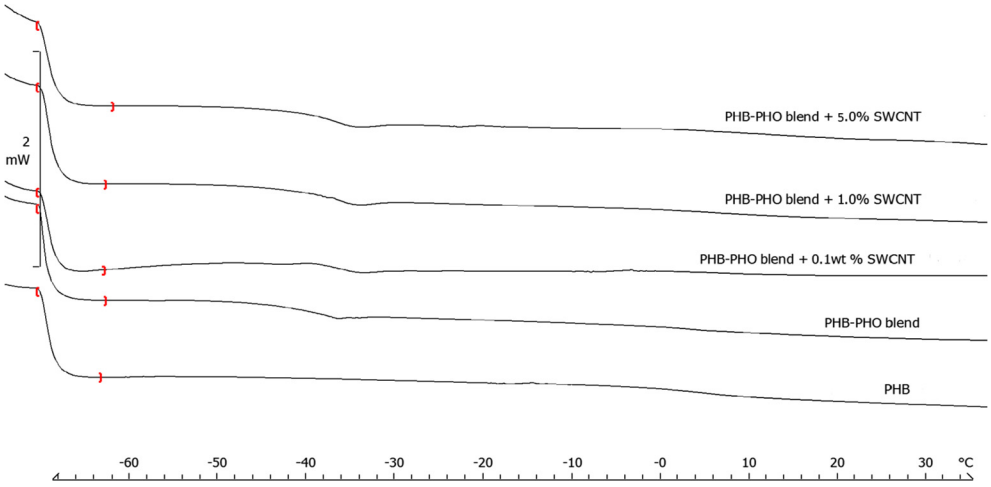

Fig. 8. DSC thermograms of second heating curves showing glass transitions around −35 °C and 3 °C for PHO and PHB phases, respectively.

Table 1
Thermal properties of equimolar PHB/PHO blends containing SWCNT.

SWCNT content in PHB/PHO blend	$T_{m(PHB)}$ (°C)	$T_{c(PHB)}$ (°C)	Crystallinity (% in PHB fraction)
0.1	170	77	50
0.5	174	82	44
1.0	173	80	44
2.5	174	87	42
5.0	174	97	46
7.5	175	96	48
10	167	92	52

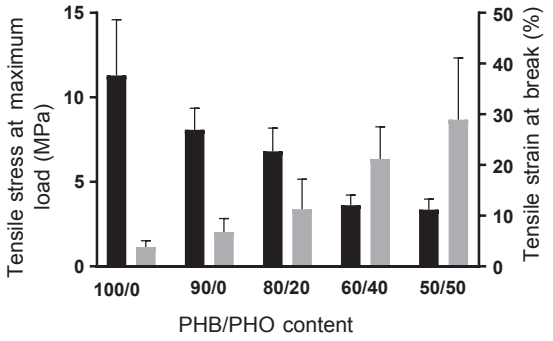

Fig. 9. Tensile properties of PHA blends (PHB/PHO). Tensile stress: black columns; Tensile strain at break: grey columns. $N = 5$, error bars represent standard error of the mean.

previously been shown to have decreased tensile stress and increased elongation at break with increasing PHO content [12,20]. In the work presented here, a gradual increase in elongation at break was observed, accompanied by decreasing tensile stress up to 50% PHO in the blended film (Fig. 9). The formation of co-continuous phases in the equimolar blend reported in the literature and shown in Figs. 1 and 5 resulted in a film with intermediate stress/strain properties, providing a suitable starting point to observe the effect of addition of SWCNT on material properties.

The tensile stress and tensile strain at break of equimolar PHB/PHO blends containing SWCNT were comparable with SWCNT loadings up to 2.5 wt%, above which the material stress and strain of the nanocomposite films were reduced considerably (Fig. 10). The network of carbon nanotubes may be interacting with the polymer chains of each phase to distribute the extension forces more evenly across the film [31,32]. The decrease in stress/strain values for blends with 5 wt% SWCNT was unexpected given the apparent increasing miscibility

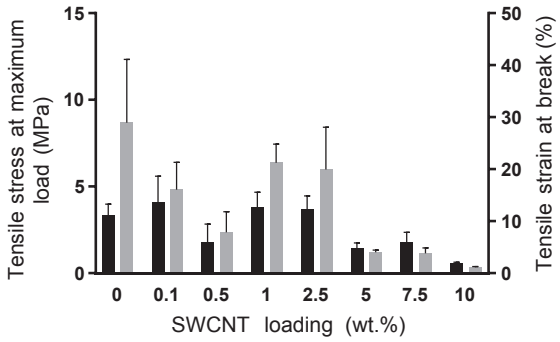

Fig. 10. Tensile properties of equimolar PHB/PHO blends containing SWCNT. Tensile stress: black columns; Tensile strain at break: grey columns. $N = 5$, error bars represent standard error of the mean.

observed by IRM and SEM. However, this may be due to aggregation of nanoparticles. Recent work using AFM-IR to characterize polymer miscibility could be useful in providing higher spatial resolution to probe phase boundaries, and characterizing the dispersion of SWCNT [30].

3.5. Assessment of nanocomposite films supporting cell growth

Olfactory Ensheathing Cells (OECs) have been experimentally shown to have potential in regeneration of spinal cord injuries and their widely investigated use has been reviewed, including applications involving tissue regeneration scaffolds [37]. OECs were used in our studies for preliminary evaluation of the suitability of the above polymer blends for future applications involving nerve regeneration. Attachment and growth of OECs on PHB/PHO film (SWCNT-free) was established after 3–5 days incubation, with many filipodiae connecting to the film surface and each other, a healthy morphological display (Fig. 11a). Growth on nanocomposite films containing 0.1–1 wt% SWCNT showed similar similar cell morphology and coverage in the same incubation period (Fig. 11b–d). However, while PHB/PHO films containing 2.5 and 5% wt% SCWNT showed some healthy cellular coverage, there were a noticeable number of stresed cells displaying more rounded, bulbous morphology (Fig. 11e and f). Surface topology in films containing 2.5 and 5 wt% SWCNT were comparatively more irregular than films with lower loadings, surface topopgraphy of biomaterials is known to influence cell attachment and coverge [38]. Similarly, surface wettability and charge may also have changed as a consequence of the SWCNT loadings [39].

Kolosnjaj-Tabi *et al.* reported that short (< 300 nm) and well

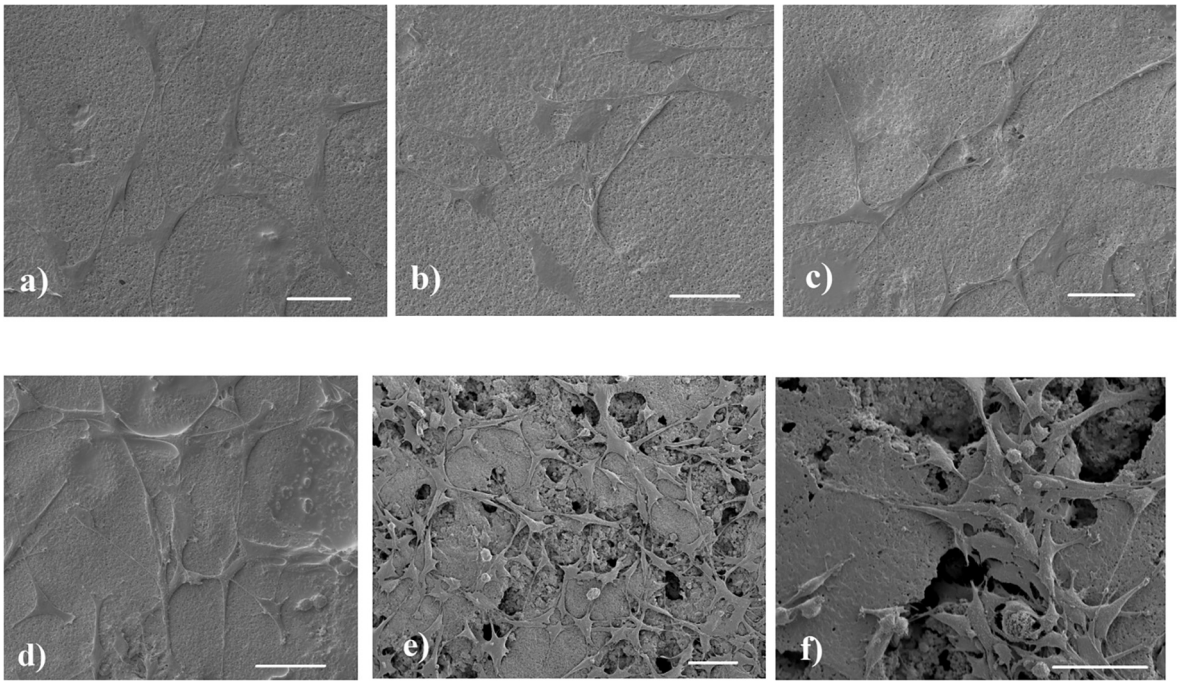

Fig. 11. SEM images of OEC growth on equimolar PHB/PHO films with SWCNT loadings: (a) 0 wt%, (b) 0.1 wt%, (c) 0.5 wt%, (d) 1 wt%, (e) 2.5 wt%, (f) 5 wt%. Bar = 50 μm.

dispersed SWCNT have been shown to pass through the reticuloendothelial system and the kidneys [40]. The choice of short SWCNT as a filler in biopolymer scaffolds may reduce the likelihood of toxicity once the scaffold undergoes biodegradation within the tissue. However, it would be necessary to assess the aggregation of nanoparticles that may occur in a physiological system during biodegradation of the biopolymer scaffold, and modification of SWCNTs may be used to inhibit aggregation or enhance uptake into the cytoplasm of macrophage cells [41].

4. Conclusions

Considering the influence of SWCNT addition on the miscibility of PHB-PHO blended films and their improved electrical conductivity, a nanocomposite film containing 1 wt% SWCNT could provide a suitable material to support OEC growth, potentially providing a suitable matrix for neural cells and the possibility to direct or enhance growth via electrical stimulation. The production of a biocompatible PHA polymer blend with desirable mechanical properties is hampered by the immiscibility of PHB and PHO, which may be alleviated by the addition of nanoparticle fillers such as SWCNT. The electrical percolation threshold in nanocomposite films was observed between 0.5 and 1 wt% SWCNT loading in PHA blends, which compares favourably with compositions that have demonstrated improved performance for mammalian cell proliferation and activity. In the design of a biomaterial to support nerve repair, material stiffness is required to permit implantation without subsequent tissue compression, while flexibility allows movement, the combination must also support maintenance of a stable electrode-tissue interface [42]. Phase separation was only partially affected by addition of SWCNT as shown by IRM and SEM, and the application of a deuterium-labelled polymer continues to prove useful in probing phase separation of polymers.

Acknowledgement

The authors thank Dr Tamim Darwish, National Deuteration Facility, ANSTO for supply of octanoic acid-d_{15}.

Author contributions

The manuscript was written through contributions of all authors. All authors have given approval to the final version of the manuscript.

Funding sources

Infrared microspectroscopy analysis was undertaken on the Infrared beamline and associated instruments at the Australian Synchrotron, Victoria, Australia.

Deuteration and preparation of films was undertaken at the National Deuteration Facility which was partly funded by the National Collaborative Research Infrastructure Strategy – an initiative of the Australian Government.

This research used the facilities supported by Australian Microscopy and Microanalysis Research Facility at the Electron Microscope Unit at UNSW.

Appendix A. Supplementary data

Supplementary data associated with this article can be found, in the online version, at https://doi.org/10.1016/j.eurpolymj.2018.05.031.

References

[1] R.W. Lenz, R.H. Marchessault, Bacterial polyesters: biosynthesis, biodegradable plastics and biotechnology, Biomacromolecules 6 (1) (2005) 1–8.
[2] M. Zinn, B. Witholt, T. Egli, Occurrence, synthesis and medical application of bacterial polyhydroxyalkanoate, Adv. Drug Deliv. Rev. 53 (1) (2001) 5–21.
[3] M. Kunioka, Y. Doi, Thermal degradation of microbial copolyesters: poly(3-hydroxybutyrate-co-3-hydroxyvalerate) and poly(3-hydroxybutyrate-co-4-hydroxybutyrate), Macromolecules 23 (7) (1990) 1933–1936.
[4] B. Laycock, P. Halley, S. Pratt, A. Werker, P. Lant, The chemomechanical properties of microbial polyhydroxyalkanoates, Progr. Polym. Sci. 38 (3–4) (2013) 536–583.
[5] E. Biazar, Polyhydroxyalkanoates as potential biomaterials for neural tissue regeneration, Int. J. Polym. Mater. Polym. Biomater. 63 (17) (2014) 898–908.
[6] G.-Q. Chen, Q. Wu, The application of polyhydroxyalkanoates as tissue engineering materials, Biomaterials 26 (33) (2005) 6565–6578.
[7] S.K. Misra, S.P. Valappil, I. Roy, A.R. Boccaccini, Polyhydroxyalkanoate (PHA)/inorganic phase composites for tissue engineering applications, Biomacromolecules 7 (8) (2006) 2249–2258.

[8] M. Martina, D.W. Hutmacher, Biodegradable polymers applied in tissue engineering research: a review, Polym. Int. 56 (2) (2007) 145–157.
[9] Z. Bartczak, A. Galeski, M. Kowalczuk, M. Sobota, R. Malinowski, Tough blends of poly(lactide) and amorphous poly([R, S]-3-hydroxy butyrate) – morphology and properties, Eur. Polym. J. 49 (11) (2013) 3630–3641.
[10] Z. Chen, S. Cheng, K. Xu, Block poly(ester-urethane)s based on poly(3-hydroxybutyrate-co-4-hydroxybutyrate) and poly(3-hydroxyhexanoate-co-3-hydroxyoctanoate), Biomaterials 30 (12) (2009) 2219–2230.
[11] T. Furukawa, H. Sato, R. Murakami, J. Zhang, Y.-X. Duan, I. Noda, S. Ochiai, Y. Ozaki, Structure, dispersibility, and crystallinity of poly(hydroxybutyrate)/poly(l-lactic acid) blends studied by FT-IR microspectroscopy and differential scanning calorimetry, Macromolecules 38 (15) (2005) 6445–6454.
[12] M. Nerkar, J.A. Ramsay, B.A. Ramsay, M. Kontopoulou, Melt compounded blends of short and medium chain-length poly-3-hydroxyalkanoates, J. Polym. Environ. 22 (2) (2014) 236–243.
[13] S.M. Martelli, J. Sabirova, F.M. Fakhoury, A. Dyzma, B. de Meyer, W. Soetaert, Obtention and characterization of poly(3-hydroxybutyricacid-co-hydroxyvaleric acid)/mcl-PHA based blends, LWT - Food Sci. Technol. 47 (2) (2012) 386–392.
[14] M.J.A. Hore, M. Laradji, Prospects of nanorods as an emulsifying agent of immiscible blends, J. Chem. Phys. 128 (5) (2008) 054901–54908.
[15] D. Wu, Y. Zhang, M. Zhang, W. Yu, Selective localization of multiwalled carbon nanotubes in poly(ε-caprolactone)/polylactide blend, Biomacromolecules 10 (2) (2009) 417–424.
[16] S. Bose, R. Cardinaels, C. Özdilek, J. Leys, J.W. Seo, M. Wübbenhorst, P. Moldenaers, Effect of multiwall carbon nanotubes on the phase separation of concentrated blends of poly[(α-methyl styrene)-co-acrylonitrile] and poly(methyl methacrylate) as studied by melt rheology and conductivity spectroscopy, Eur. Polym. J. 53 (2014) 253–269.
[17] A. Nuzzo, E. Bilotti, T. Peijs, D. Acierno, G. Filippone, Nanoparticle-induced co-continuity in immiscible polymer blends – a comparative study on bio-based PLA-PA11 blends filled with organoclay, sepiolite, and carbon nanotubes, Polymer 55 (19) (2014) 4908–4919.
[18] J. Huang, C. Mao, Y. Zhu, W. Jiang, X. Yang, Control of carbon nanotubes at the interface of a co-continuous immiscible polymer blend to fabricate conductive composites with ultralow percolation thresholds, Carbon 73 (2014) 267–274.
[19] J.K.W. Sandler, J.E. Kirk, I.A. Kinloch, M.S.P. Shaffer, A.H. Windle, Ultra-low electrical percolation threshold in carbon-nanotube-epoxy composites, Polymer 44 (19) (2003) 5893–5899.
[20] A. Dufresne, M. Vincendon, Poly(3-hydroxybutyrate) and poly(3-hydroxyoctanoate) blends: morphology and mechanical behavior, Macromolecules 33 (8) (2000) 2998–3008.
[21] R.A. Russell, T.A. Darwish, L. Puskar, D.E. Martin, P.J. Holden, L.J.R. Foster, Deuterated polymers for probing phase separation using infrared microspectroscopy, Biomacromolecules 15 (2) (2014) 644–649.
[22] A. Fabbro, A. Villari, J. Laishram, D. Scaini, F.M. Toma, A. Turco, M. Prato, L. Ballerini, Spinal cord explants use carbon nanotube interfaces to enhance neurite outgrowth and to fortify synaptic inputs, ACS Nano 6 (3) (2012) 2041–2055.
[23] T. Gordon, O.A.R. Sulaiman, A. Ladak, G. Stefano, T. Pierluigi, B. Bruno, Chapter 24 electrical stimulation for improving nerve regeneration: where do we stand? in: International Review of Neurobiology, vol. 87, Academic Press, 2009, pp. 433–444.
[24] S.H. Jeong, S.B. Jun, J.K. Song, S.J. Kim, Activity-dependent neuronal cell migration induced by electrical stimulation, Med. Biol. Eng. Comput. 47 (1) (2009) 93–99.
[25] B. Sun, T. Wu, J. Wang, D. Li, J. Wang, Q. Gao, M.A. Bhutto, H. El-Hamshary, S.S. Al-Deyab, X. Mo, Polypyrrole-coated poly(l-lactic acid-co-ε-caprolactone)/silk fibroin nanofibrous membranes promoting neural cell proliferation and differentiation with electrical stimulation, J. Mater. Chem. B 4 (41) (2016) 6670–6679.
[26] L. Yan, B. Zhao, X. Liu, X. Li, C. Zeng, H. Shi, X. Xu, T. Lin, L. Dai, Y. Liu, Aligned nanofibers from polypyrrole/graphene as electrodes for regeneration of optic nerve via electrical stimulation, ACS Appl. Mater. Interfaces 8 (11) (2016) 6834–6840.
[27] R.A. Russell, P.J. Holden, K.L. Wilde, K.M. Hammerton, L.J.R. Foster, Production and use of deuterated polyhydroxyoctanoate in structural studies of PHO inclusions, J. Biotechnol. 132 (3) (2007) 303–305.
[28] L.J.R. Foster, R.A. Russell, V. Sanguanchaipaiwong, D.J.M. Stone, J.M. Hook, P.J. Holden, Biosynthesis and characterization of deuterated polyhydroxyoctanoate, Biomacromolecules 7 (4) (2006) 1344–1349.
[29] P.J. Barham, A. Keller, E.L. Otun, P.A. Holmes, Crystallization and morphology of a bacterial thermoplastic: poly-3-hydroxybutyrate, J. Mater. Sci. 19 (9) (1984) 2781–2794.
[30] M.A. Rickard, G.F. Meyers, B.M. Habersberger, C.W. Reinhardt, J.J. Stanley, Nanoscale chemical imaging of a deuterium-labeled polyolefin copolymer in a polyolefin blend by atomic force microscopy-infrared spectroscopy, Polymer 129 (Suppl. C) (2017) 247–251.
[31] J.S.F. Barrett, A.A. Abdala, F. Srienc, Poly(hydroxyalkanoate) elastomers and their graphene nanocomposites, Macromolecules 47 (12) (2014) 3926–3941.
[32] C. Vallejo-Giraldo, E. Pugliese, A. Larrañaga, M.A. Fernandez-Yague, J.J. Britton, A. Trotier, G. Tadayyon, A. Kelly, I. Rago, J.-R. Sarasua, E. Dowd, L.R. Quinlan, A. Pandit, M.J.P. Biggs, Polyhydroxyalkanoate/carbon nanotube nanocomposites: flexible electrically conducting elastomers for neural applications, Nanomedicine 11 (19) (2016) 2547–2563.
[33] L.-P. Wu, M. You, D. Wang, G. Peng, Z. Wang, G.-Q. Chen, Fabrication of carbon nanotube (CNT)/poly(3-hydroxybutyrate-co-3-hydroxyhexanoate) (PHBHHx) nanocomposite films for human mesenchymal stem cell (hMSC) differentiation, Polym. Chem. 4 (16) (2013) 4490–4498.
[34] J.M. García-García, M.M. Bernal, R. Verdejo, M.A. López-Manchado, E. Doncel-Pérez, L. Garrido, I. Quijada-Garrido, Semiconductive bionanocomposites of poly(3-hydroxybutyrate-co-3-hydroxyhexanoate) and MWCNTs for neural growth applications, J. Polym. Sci. Part B: Polym. Phys. 52 (5) (2014) 349–360.
[35] A. Dufresne, M. Paillet, J.L. Putaux, R. Canet, F. Carmona, P. Delhaes, S. Cui, Processing and characterization of carbon nanotube/poly(styrene-co-butyl acrylate) nanocomposites, J. Mater. Sci. 37 (18) (2002) 3915–3923.
[36] L. Valentini, P. Fabbri, M. Messori, M. Degli Esposti, S. Bittolo Bon, Multilayer films composed of conductive poly(3-hydroxybutyrate)/carbon nanotubes bionanocomposites and a photoresponsive conducting polymer, J. Polym. Sci. Part B: Polym. Phys. 52 (8) (2014) 596–602.
[37] I. Vismara, S. Papa, F. Rossi, G. Forloni, P. Veglianese, Current options for cell therapy in spinal cord injury, Trends Mol. Med. 23 (9) (2017) 831–849.
[38] D. Daranarong, B. Thapsukhon, N.S. Wanandy, R. Molloy, W. Punyodom, L.J.R. Foster, Application of low loading of collagen in electrospun poly [(l-lactide)-co-(ε-caprolactone)] nanofibrous scaffolds to promote cellular biocompatibility, Polym. Int. 63(7) (2014) 1254–1262.
[39] L.J.R. Foster, B.J. Tighe, Centrifugally spun polyhydroxybutyrate fibres: accelerated hydrolytic degradation studies, Polym. Degrad. Stab. 87 (1) (2005) 1–10.
[40] J. Kolosnjaj-Tabi, K.B. Hartman, S. Boudjemaa, J.S. Ananta, G. Morgant, H. Szwarc, L.J. Wilson, F. Moussa, In vivo behavior of large doses of ultrashort and full-length single-walled carbon nanotubes after oral and intraperitoneal administration to Swiss mice, ACS Nano 4 (3) (2010) 1481–1492.
[41] A.E. Porter, M. Gass, J.S. Bendall, K. Muller, A. Goode, J.N. Skepper, P.A. Midgley, M. Welland, Uptake of noncytotoxic acid-treated single-walled carbon nanotubes into the cytoplasm of human macrophage cells, ACS Nano 3 (6) (2009) 1485–1492.
[42] R.T. Hassarati, L.J.R. Foster, R.A. Green, Influence of biphasic stimulation on olfactory ensheathing cells for neuroprosthetic devices, Front. Neurosci. 10 (432) (2016) 1–11.